Inorganic Chemistry

Article

pubs.acs.org/IC

Precursor Routes to Complex Ternary Intermetallics: Single-Crystal and Microcrystalline Preparation of Clathrate-I $Na_8Al_8Si_{38}$ from NaSi + NaAlSi

Yongkwan Dong,[†] Ping Chai,[†] Matt Beekman,*[,‡] Xiaoyu Zeng,[§] Terry M. Tritt,[§] and George S. Nolas*[,†]

[†]Department of Physics, University of South Florida, Tampa, Florida 33620, United States

[‡]Department of Natural Sciences, Oregon Institute of Technology, Klamath Falls, Oregon 97601, United States

[§]Department of Physics and Astronomy, Kinard Laboratory, Clemson University, Clemson, South Carolina 29634, United States

Supporting Information

ABSTRACT: Single crystals of the ternary clathrate-I $Na_8Al_8Si_{38}$ were synthesized by kinetically controlled thermal decomposition (KCTD), and microcrystalline $Na_8Al_8Si_{38}$ was synthesized by spark plasma sintering (SPS) using a NaSi + NaAlSi mixture as the precursor. $Na_8Al_xSi_{46-x}$ compositions with $x \leq 8$ were also synthesized by SPS from precursor mixtures of different ratios. The crystal structure of $Na_8Al_8Si_{38}$ was investigated using both Rietveld and single-crystal refinements. Temperature-dependent transport and UV/vis measurements were employed in the characterization of $Na_8Al_8Si_{38}$, with diffuse-reflectance measurement indicating an indirect optical gap of 0.64 eV. Our results indicate that, when more than one precursor is used, both SPS and KCTD are effective methods for the synthesis of multinary inorganic phases that are not easily accessible by traditional solid-state synthesis or crystal growth techniques.

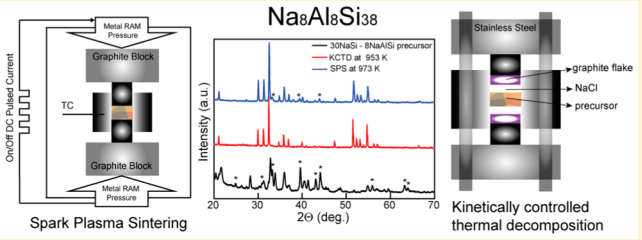

INTRODUCTION

Group 14 intermetallic clathrates have been extensively investigated because of their distinctive structural and physical properties.[1−4] The group 14 clathrate-I structure, with chemical formula A_8X_{46}, is composed of a three-dimensional open framework of face-sharing X_{20} dodecahedra and X_{24} tetrakaidekahedra where "guest" atoms, A, reside. Typically, these guest atoms are alkali, alkaline earth, or rare earth metals or halogens.[4] The stoichiometric A_8X_{46} compositions display metallic electrical conductivity as a result of the electrons donated from the A atoms to the sp^3-hybridized group 14 framework. However, framework substitution by triel elements (group 13) or transition metals is possible, and ternary clathrate-I compounds can exhibit metallic, semiconducting, superconducting, or insulating behavior depending on the substitutional atom and the occupation fraction of the group 14 atoms and/or vacancies in the framework. These variants are of interest for technological applications including photovoltaic, thermoelectric, and magnetocaloric energy conversion, as well as superconductivity.[4−8]

Despite the scientific and technological importance of these materials, a significant number of conceivable compositions have yet to be experimentally realized, presumably because they are not the most thermodynamically stable product or are otherwise difficult to synthesize. Indeed, nearly all known ternary compositions correspond to the most thermodynamically stable phases, as the preparation of metastable variants is precluded by the formation of stable binary intermediates during the conventional solid-state reactions typically used to prepare these materials. To overcome the limited access provided by conventional synthesis methods and to obtain targeted thermodynamically metastable or otherwise difficult-to-access compositions, a variety of new synthetic techniques have recently been developed.[4] To date, these methods have primarily been used to prepare binary clathrates. One such method, kinetically controlled thermal decomposition (KCTD), allows for selective crystal growth from appropriate alkali-metal-rich binary precursors through changes in the reaction temperature.[2,9] Another synthetic approach, spark plasma sintering (SPS), is a method whereby a pulsed direct current is the primary driver of the reaction. SPS is well-known for the consolidation of ceramics, polymers, semiconductors, and nanocomsites;[10] however, the direct synthesis and crystal growth of new complex materials by SPS is still relatively rare. Recently, the binary clathrate $Na_{24}Si_{136}$ was synthesized by SPS in the form of single crystals from a NaSi precursor.[11] The selective synthesis of binary Na−Si clathrate-I and -II crystals was also achieved by adjusting the SPS temperature and pressure.[12]

In the present study, we have extended the emerging precursor-based SPS and KCTD synthetic approaches to ternary systems. Specifically, we demonstrate that both of these approaches can be applied to synthesize the new ternary

Received: February 15, 2015
Published: May 18, 2015

DOI: 10.1021/acs.inorgchem.5b00348
Inorg. Chem. 2015, 54, 5316−5321

intermetallic clathrate $Na_8Al_8Si_{38}$ using a finely divided mixture of the crystalline compounds NaSi and NaAlSi as the Na-rich precursor. Whereas ternary clathrate-I compositions $A_8Al_8Si_{38}$ with A = K, Rb or Cs were very recently prepared by conventional solid-state synthesis techniques[5] or by a combination of arc-melting, ball-milling, and reactive-flux methods,[13] $Na_8Al_8Si_{38}$ until now has not been reported, presumably because $Na_8Al_8Si_{38}$ is kinetically stable and/or cannot be synthesized by conventional methods for other reasons. In addition to demonstrating two new precursor synthetic pathways for the synthesis of ternary intermetallic compositions by SPS and KCTD, we also report both the structural and compositional characterization and the transport and optical properties of $Na_8Al_8Si_{38}$.

EXPERIMENTAL SECTION

Syntheses. $Na_8Al_xSi_{46-x}$ (x = 4, 6, 8) compounds were synthesized by SPS from a NaSi/NaAlSi precursor mixture. All preparation steps were carried out in a N_2-filled glovebox to prevent contamination or oxidation of the starting materials. To obtain an intimate mixture of the elements (and the resulting precursor phases), Al and Si were first combined in the appropriate atomic ratio and arc-melted. The resulting heterogeneous Al−Si mixture was then ground into fine powder. Each Al−Si mixture was loaded in a tungsten crucible with Na in the appropriate stoichiometric ratio (e.g., 8Al−38Si + 30Na → 8NaAlSi + 30NaSi) before the crucible was loaded into a stainless steel canister and tightly sealed. This canister was in turn placed inside a quartz tube, sealed under a vacuum, and then held at 923 K for 24 h. The resulting product was ground thoroughly and used as the precursor in SPS and KCTD reactions.

For SPS processing, the NaSi/NaAlSi mixture was loaded into a graphite die assembly inside a N_2-filled glovebox, because of the air sensitivity of NaSi. To provide a tight fit of the die assembly (to minimize Na evaporation) and to prevent direct reaction of the precursor with the die or punches, tantalum foil was placed between the precursor mixture and the graphite die and punches. After this assembly had been mounted into the SPS reaction chamber, the chamber was evacuated and flushed three times with high-purity N_2. The SPS process was performed under a dynamic vacuum (10^{-3} Torr), a uniaxial pressure of 100 MPa, and a pulsed dc current with pulse-on and -off times of 36 and 2 ms, respectively. A temperature ramp rate of 25 K/min was used to reach the desired temperature (973 K for the formation of $Na_8Al_8Si_{38}$), after which this temperature was held for 3 h. After the reaction, the current and pressure were released, and the graphite tooling was cooled to room temperature under a vacuum. The product of the reaction was separated from any unreacted NaSi by carefully washing with ethanol and distilled water.[11] (***Caution:*** *NaSi can react violently with water.*)

Single crystals of $Na_8Al_8Si_{38}$ were grown by the KCTD technique. The precursor, described above, was placed in custom-designed stainless steel tooling under a uniaxial pressure of 20 MPa and heated at 953 K for 9 h under a dynamic vacuum of 10^{-6} Torr. Phase-pure $Na_8Al_8Si_{38}$ in the form of single crystals was obtained by the slow controlled removal of Na from the NaSi/NaAlSi precursor by the vapor-phase interaction with a graphite flake, which was spatially separated from the precursor mixture using NaCl to avoid the direct solid-state reaction of the graphite and precursor. The procedure closely follows that previously reported for growth of Na−Si clathrates.[9a] After completion of the reaction, the product was washed with ethanol and distilled water and dried in air, revealing small shiny crystals.

Powder X-ray Diffraction and Elemental Analyses. Powder X-ray diffraction (PXRD) data were collected with a Bruker D8 Focus diffractometer in Bragg−Brentano geometry using Cu Kα radiation and a graphite monochromator. Structure refinements were accomplished by the Rietveld method using the GSAS suite of programs.[14] Energy-dispersive X-ray (EDX) analysis was accomplished with a scanning electron microscope (SEM, JEOL JSM-6390LV) equipped with an Oxford Instruments INCA X-Sight 7582 M unit. EDX spectroscopy and PXRD were used to examine the purities and chemical compositions of the specimens.

Single-Crystal X-ray Diffraction. Single-crystal XRD data were collected using a Bruker D8 Venture PHOTON 100 CMOS system equipped with a Cu Kα INCOATEC Imus microfocus source (λ = 1.54178 Å). The initial cubic cell constants and orientation matrix were obtained using APEX2 (difference vectors method).[15] Data integration and reduction were performed using SaintPlus 6.01.[16] An empirical absorption correction was performed by a multiscan method implemented in SADABS.[17] The initial input files for solving the crystal structure were prepared by XPREP implemented in APEX2.[15] The structure was solved using SHELXS-97 (direct methods)[18] and refined using SHELXL-97 (full-matrix least-squares techniques)[18] contained in the WinGX program package.[19]

Transport Property Measurements. Values of the high-temperature thermal conductivity, κ, were determined using the equation $\kappa = DdC_p$, where D is the measured density obtained from the specimen's measured mass and geometry, d is the measured thermal diffusivity, and C_p is the estimated heat capacity in the Dulong−Petit limit. Thermal diffusivity measurements employed the laser flash method in a flowing Ar environment with a NETZSCH LFA 457 system. The uncertainty in the thermal diffusivity measurements was ∼10%. Heat capacity $C_p(\approx C_v)$ was estimated in the Dulong−Petit limit ($C_p = 3nR$, where n is the number of atoms per formula unit and R is the ideal gas constant). The high-temperature Seebeck coefficient, S, and electrical resistivty, ρ, were measured on parallelepipeds, cut from the hot pressed pellets, with an ULVAC ZEM-3 system (experimental uncertainty of 5−10% for S and ρ at elevated temperatures). The S and ρ measurements were performed perpendicular to the pressing axis, whereas the laser flash diffusivity measurements were carried out on the entire pellet parallel to the pressing axis.

Solid-State UV/Vis Spectroscopy. Optical diffuse-reflectance measurements were performed at room temperature using a JASCO V-670 UV/vis double-beam spectrophotometer equipped with a 60-mm-diameter integrating sphere. A fine powder was prepared by grinding the polycrystalline sample. The powder was then pressed onto the sample holder. Reflectance data were collected in the wavelength range of 200−2500 nm, and absorption data were calculated from the reflectance data using the Kubelka−Munk function $\alpha/S = (1 - R)^2/2R$, where α is the absorption coefficient, S is the scattering coefficient, and R is the reflectance at a given wavelength.[20] The optical band gap was determined as the intersection point between the energy axis at the absorption offset and the line extrapolated from the linear portion of the absorption edge.

RESULTS AND DISCUSSION

During KCTD, Na is consumed by vapor-phase reaction with the spatially separated graphite, driving the decomposition of the precursor in a controlled manner.[9a] In the case of the SPS reaction of NaSi to form $Na_{24}Si_{136}$, the conversion of precursor to product is thought to be electrochemical in nature.[9b,11] Na is removed by electrically driven mass transport during SPS and is then reduced at the cathode. For the application of either of these approaches, the formation of a target phase through the precursor route first requires identification of appropriate precursors containing the constituent atoms (and preferably only those atoms). Because we could not identify an appropriate single precursor with the correct Al/Si ratio to synthesize $Na_8Al_8Si_{38}$, we chose to investigate a finely divided mixture of binary NaSi[21] and ternary NaAlSi.[22] Precursor mixtures of NaSi and $NaAlH_4$ were also tried and could be used to successfully prepare the title compound; however, the reaction was extremely energetic (explosive) and difficult to control and often damaged the SPS and KCTD tooling. Broader peaks in the powder X-ray diffraction patterns from the

DOI: 10.1021/acs.inorgchem.5b00348
Inorg. Chem. 2015, 54, 5316−5321

products of reactions of NaSi with $NaBH_4$ also indicated a significant homogeneity range.

In a physical mixture of NaSi and NaAlSi, the correct Al/Si ratio can readily be controlled, although the overall composition will necessarily be Na-rich compared to the composition $Na_8Al_8Si_{38}$. The crystal structures of the precursor compounds are shown in Figure 1. NaSi, which contains

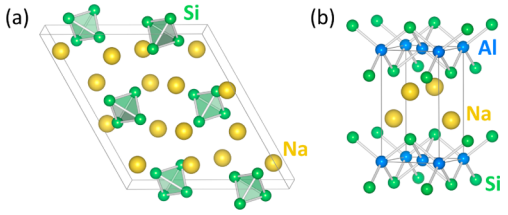

Figure 1. Crystal structures of (a) NaSi and (b) NaAlSi.

isolated $[Si_4]^{4-}$ polyanions and mobile Na^+ cations, has been employed as an effective precursor for synthesis of binary Na–Si clathrates by KCTD and SPS.[9a,11] The layered crystal structure of NaAlSi also contains Na^+ cations that can also be expected to be mobile, whereas Al is tetrahedrally coordinated by Si in infinite two-dimensional layers, with local coordination similar to that in the $Na_8Al_8Si_{38}$ framework. We note that, as is also the case with conventional thermal decomposition of alkali tetrelide precursors,[4] the detailed reaction pathways underlying the conversion of the precursor to products in SPS and KCTD are not yet completely understood.

Figure 2 shows the PXRD patterns of the NaSi/NaAlSi starting precursor mixture and the KCTD- and SPS-prepared

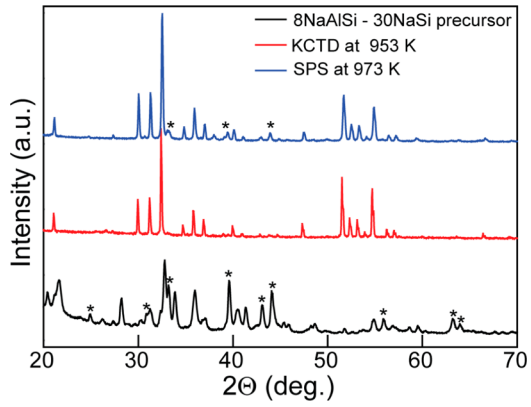

Figure 2. PXRD patterns of the precursor and products for each reaction. Asterisks indicate the peaks from the NaAlSi phase, with all other reflections in the precursor pattern corresponding to NaSi. The PXRD pattern of the KCTD product was obtained from crushed single crystals.

$Na_8Al_8Si_{38}$ specimens. We observed no evidence for the formation of any clathrate phase in the precursor mixture, indicating that the clathrate phase either is not the most thermodynamically stable product at this particular Na–Al–Si composition or is kinetically hindered from forming under these reaction conditions. The resulting KCTD specimen was phase-pure, whereas the SPS specimen contained a small amount of unreacted NaAlSi.

Small single crystals were obtained by the KCTD synthetic method. Crystallographic details and data collection for both powder and single-crystal refinements of $Na_8Al_8Si_{38}$ are provided in Table 1, and selected bond distances of the framework are listed in Table 2. The partial crystal structure is

Table 1. Crystallographic Details for $Na_8Al_8Si_{38}$

	Rietveld	single crystal
space group, Z		$Pm\bar{3}n$ (No. 223), 1
a (Å)	10.3260(1)	10.3170(1)
V (Å^3)	1101.03(5)	1098.15(2)
radiation	graphite-monochromated Cu Kα (1.54056 Å)	Cu Kα INCOATEC Imus microfocus source (λ = 1.54178 Å)
T (K)	298	100
absorption coefficient (mm^{-1})		12.725
D_{calc} (g/cm^3)	2.218	2.219
θ limits (deg)	7.5–50.04	6.07–72
no. of unique data with F_o^2		6231/220 [R(int) = 0.0399]
no. of unique data with $F_o^2 > 2\sigma(F_o^2)$		201
R indices	0.1217, 0.0993 (wRp, Rp)[a]	0.0348, 0.0130 (wR2, R1)[b]
goodness of fit on F^2	3.66	1.108
max and min residual electron densities (e/Å^3)		0.260 and −0.152

[a] wRp = $\{[\sum w(I_o - I_c)^2]/\sum wI_o^2\}^{1/2}$ and Rp = $(\sum|I_o - I_c|)/\sum I_o$. [b] wR2 ($F_o^2 > 0$) and R1 [$F_o^2 > 2\sigma(F_o^2)$].

Table 2. Selected Bond Distances (Å) for $Na_8Al_8Si_{38}$

	Rietveld	single crystal
Si1/Al1–Si3/Al3 × 4	2.43407(3)	2.4505(5)
Si2–Si2	2.358(8)	2.3549(1)
Si2–Si3/Al3 × 3	2.3823(13)	2.3742(3)
Si3/Al3–Si3/Al3	2.41003(4)	2.3883(9)

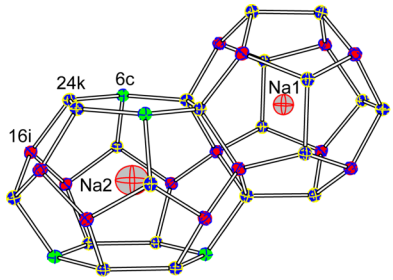

Figure 3. Partial crystal structure of $Na_8Al_8Si_{38}$ illustrating all crystallographic sites and their local environments. Na1 (2a) and Na2 (6d) reside at the centers of a dodecahedron and a tetrakaidecahedron, respectively. Al and Si share the 6c (green, 0.79/0.21) and 24k (blue, 0.13/0.87) crystallographic sites, whereas only Si2 is on the 16i crystallographic site. Atomic displacement parameters are shown for 99% probability.

illustrated in Figure 3. The refined unit-cell parameters and bond distances of $Na_8Al_8Si_{38}$ are larger than those of Na_8Si_{46} [a = 10.1962(9) Å][9a] because of the inclusion of Al in the framework but smaller than those of $A_8Al_8Si_{38}$ (A = K, Rb, Cs)[5,13] and $Ba_8Al_8Si_{38}$[23] because of the smaller ionic size of the encapsulated Na atoms. Indeed, a plot of the lattice parameter as a function of the ionic radius (coordination number CN = 12)[24] for $A_8Al_8Si_{38}$ (A = Na, K, Rb, Cs, and Ba) is relatively well described by a linear relationship (Figure 4). Although the

DOI: 10.1021/acs.inorgchem.5b00348
Inorg. Chem. 2015, 54, 5316–5321

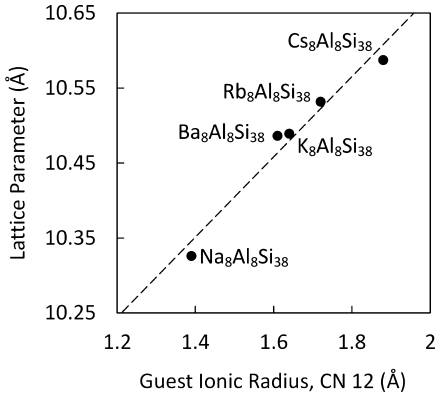

Figure 4. Plot of lattice parameter versus ionic radius [coordination number (CN) = 12] of the guest atoms for $A_8Al_8Si_{38}$ (A = Na, K, Rb, Cs, and Ba).[13,23]

accuracy of compositions obtained by EDX spectroscopy without the use of internal standards is lower than that with the use of standards, the $Na_8Al_8Si_{38}$ composition was qualitatively corroborated by EDX analyses, with an average Na/Al/Si ratio of 7.8(4)/8.1(3)/38.0(6) calculated from 12 random points of four different crystals analyzed semi-quantitatively. $Na_8Al_8Si_{38}$ is cubic with the space group $Pm\bar{3}n$. The Al and Si atoms are located at the 6*c*, 16*i*, and 24*k* crystallographic sites to form two types of covalently bonded polyhedra, namely, two dodecahedra, X_{20}, and six tetrakaidecahedra, X_{24} (X = Al, Si), encapsulating Na1 and Na2 at the 2*a* and 6*d* crystallographic sites, respectively, as shown in Figure 3. Site occupancy refinement for both the guest atom and framework crystallographic sites found both to be fully occupied. The framework sites are shared between Al and Si atoms. The Al/Si ratios refined to the values 0.79/0.21 for the 6*c* site and 0.13/0.87 for the 24*k* site, whereas the 16*i* site is fully occupied by only Si atoms.[5,23] However, because of the weak X-ray scattering contrast between the neighboring elements Si and Al, we cannot definitively assign the site occupancies for Al on the framework by conventional XRD. Na1 and Na2 atoms fully occupy the interstitial 2*a* and 6*d* sites. The refined occupancies, atomic coordinates, and equivalent (U_{eq}) and anisotropic (U_{ij}) atomic displacement parameters can be found in the Supporting Information (CIF).

Figure 5 shows the powder XRD patterns of $Na_8Al_8Si_{38}$ specimens synthesized at different SPS temperatures. NaAlSi did not react completely at 873 K, whereas the amount of α-Si

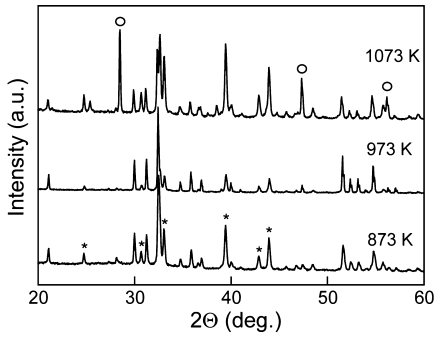

Figure 5. PXRD patterns of materials with different NaSi/NaAlSi ratios obtained at different SPS processing temperatures. Asterisks indicate NaAlSi, and open circles indicate α-Si.

was high at 1073 K, potentially due to decomposition of $Na_8Al_8Si_{38}$. The latter case indicates that the decomposition rate of the product is comparable to the reaction rate between NaAlSi and NaSi. Nevertheless, this illustrates the optimal conditions for the synthesis of $NaAl_xSi_{46-x}$. With this in mind, we varied x (Figure 6) in an attempt to synthesize different

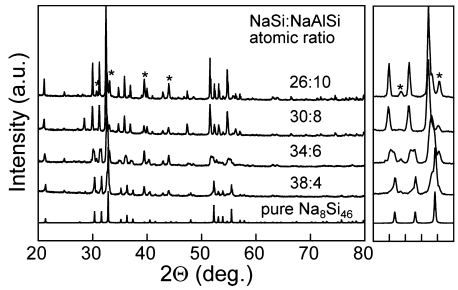

Figure 6. PXRD patterns of SPS-synthesized $Na_8Al_xSi_{38-x}$ materials with different NaSi/NaAlSi ratios. $Na_8Al_4Si_{42}$ was obtained at 773 K, and $Na_8Al_6Si_{40}$ was obtained at 873 K. Asterisks indicate unreacted NaAlSi.

clathrate compositions starting from the appropriate NaSi/NaAlSi precursor ratios. The main peaks between 29° and 34° in Figure 6 appeared to shift to lower angle with increasing NaAlSi content (corresponding to increased Al content in the framework and a larger lattice parameter). However, the peaks did not shift any further even when the NaAlSi content was increased such that the nominal composition had $x > 8$. These results indicate that the Al content in $Na_8Al_xSi_{46-x}$ is controllable up to $x = 8$ by this SPS process, although the broad features in the powder XRD patterns for $0 < x < 8$ suggest that these specimens might contain multiple clathrate phases of slightly different Al contents and that the preparation conditions for compositions with $0 < x < 8$ have not been optimized.

The UV/vis diffuse-reflectance spectrum is shown in Figure 7 and indicates an optical band gap of 0.64 eV. This is somewhat

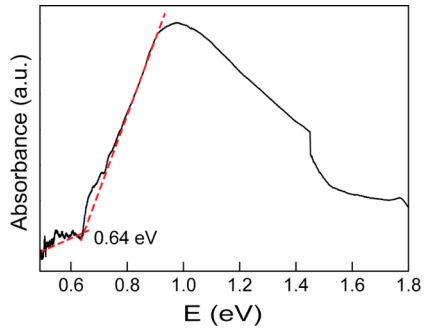

Figure 7. Solid-state UV/vis absorption spectrum of $Na_8Al_8Si_{38}$. A value of 0.64 eV for the optical band gap was obtained from the intersection of the fitted baseline and the absorption edge (red dotted line).

smaller than the (unadjusted) theoretical indirect gap of the hypothetical guest free Si_{46} (0.7 eV)[25] and α-Ge (0.74 eV),[26] noting that density functional theory typically underestimates the electronic band gap for most materials. In comparison, $K_8Al_8Si_{38}$ was reported to have an experimental direct band gap of 1.29 eV and an indirect band gap of 1.06 eV, whereas $K_8Ga_8Si_{38}$ has much smaller direct and indirect gaps of 0.27 and

DOI: 10.1021/acs.inorgchem.5b00348
Inorg. Chem. 2015, 54, 5316−5321

0.10 eV, respectively.[5,27] The broad absorbance edge near the band gap suggests that $Na_8Al_8Si_{38}$ has an indirect band gap, similarly to Si_{46},[25] $K_8Al_8Si_{38}$,[5] and $K_8Ga_8Si_{38}$.[27] The band gap is believed to originate mainly from transitions involving filled hybridized 3s and 3p Al and Si states in the valence band and empty Al and Si 3s and 3p hybridized orbitals in the conduction band. If the contributions from Na ions near the Fermi level are minimal due to their strong ionic bonding character with the Al_8Si_{38} framework, the size of the band gap would be expected to be determined by the Al_8Si_{38} framework. First principles calculations may provide insight into the reasons for the differing band gaps of $Na_8Al_8Si_{38}$ and $K_8Al_8Si_{38}$.

The temperature-dependent electrical conductivity (σ), obtained from the measured electrical resistivity, ρ, and Seebeck coefficient, S, are shown in Figure 8a. The value of σ

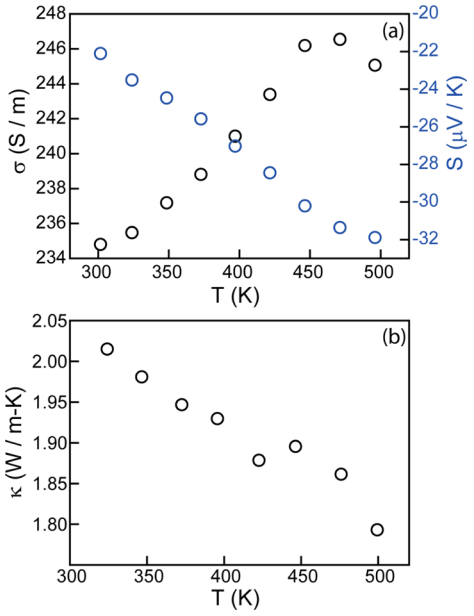

Figure 8. Temperature-dependent vcalues of (a) σ (black circles) and S (blue circles) and (b) κ for $Na_8Al_8Si_{38}$.

and modulus of S both increase with increasing temperature, and the negative S values throughout the entire measured temperature range imply electron conduction. The relatively weak activated temperature dependence of σ reflects an activation energy on the order of several millielectronvolts, significantly smaller than $E_g/2 = 0.32$ eV. This suggests that the conduction electrons originate from donor states. The room-temperature S value (−22 μV/K) is smaller than that of $A_8Al_8Si_{38}$ (A = K, Rb, Cs)[13] and comparable to those of other Al-containing clathrate-I compounds such as $Ba_8Al_{14}Si_{31}$ (−21 μV/K)[27] and $Ba_8Al_{16}Si_{30}$ (−48 μV/K).[28] Although our single-crystal diffraction refinements and EDS measurements do not allow us to quantify the aluminum content precisely, our electrical transport data suggest that the value of x in our $Na_8Al_{8-x}Si_{38}$ sample might be slightly less than 8. From a simple crystal chemical formulation, the chemical formula can be written as $[Na^+]_8[(4b)Al^-]_x[(4b)Si^0]_{46-x}\cdot(8-x)e^-$. For x = 8, intrinsic semiconducting behavior can be expected. For $x < 8$, the additional electrons originating from the Na guests do not participate in Al−Si covalent bonding and can be readily promoted to the conduction band from shallow donor states, resulting in a high carrier density.

The measured κ values are shown in Figure 8b and decrease with increasing temperature, typical of dielectric behavior. Using the measured electrical conductivity and the Wiedemann−Franz law, $\kappa_e = L_0\sigma T$ ($L_0 = 2.45 \times 10^{-8}$ W Ω K^{-2}), the electronic contribution κ_e to the thermal conductivity is estimated to be significantly less than 1% of the total thermal conductivity at all temperatures. The room-temperature κ value (2.0 W m^{-1} K^{-1}) is slightly larger than that of $A_8Al_8Si_{38}$ (A = K, Rb, Cs),[13] but much smaller than that of Na_8Si_{46}, which exhibits metallic conduction.[29]

CONCLUSIONS

Ternary $Na_8Al_xSi_{46-x}$ clathrate-I compounds with different x values up to x = 8 were synthesized by SPS, and $Na_8Al_8Si_{38}$ single crystals were synthesized by KCTD using a precursor that was a mixture of NaSi and NaAlSi for both synthetic methods. Both Rietveld and single-crystal refinements for $Na_8Al_8Si_{38}$ indicated that Al and Si share the crystallographic 6*c* and 24*k* sites with occupancy ratios of 0.79/0.21 and 0.13/0.87, respectively, whereas the crystallographic 16*i* site is occupied by only Si atoms. Transport properties of $Na_8Al_8Si_{38}$ indicate semiconducting behavior. Solid-state UV/vis diffuse-reflectance measurements indicate that $Na_8Al_8Si_{38}$ exhibits an indirect optical band gap of 0.64 eV. Our results indicate that both the SPS and KCTD synthetic methods can be employed for the synthesis of targeted multinary inorganic phases that cannot be accessible by traditional crystal growth techniques, provided that appropriate precursors can be identified. Sui et al.[31] reported the synthesis and transport properties of $A_8M_8Si_{38}$ compositions with A = K, Rb, and Cs and M = Al and Ga. The thermal conductivities of these compounds are comparable to the values observed for $Na_8Al_8Si_{38}$. Imai et al.[32] reported the successful synthesis of $K_8Al_8Si_{38}$ by direct reaction of the elements; however, $Na_8Al_xSi_{46-x}$, with a small Al content (x = 0.5), could be prepared only by high-pressure, high-temperature methods and could not be produced as the phase-pure product. These reports further corroborate the conclusion that $Na_8Al_8Si_{38}$ is not readily prepared by conventional solid-state synthesis techniques.

ASSOCIATED CONTENT

Supporting Information

Crystallographic cif file for $Na_8Al_8Si_{38}$. The Supporting Information is available free of charge on the ACS Publications website at DOI: 10.1021/acs.inorgchem.5b00348.

AUTHOR INFORMATION

Corresponding Authors

*E-mail: matt.beekman@oit.edu (M.B.).
*E-mail: gnolas@usf.edu (G.S.N.).

Author Contributions

Y.D. and P.C. contributed equally to this work.

Notes

The authors declare no competing financial interest.

ACKNOWLEDGMENTS

Y.D., P.C., and G.S.N. gratefully acknowledge support from the U.S. Department of Energy, Basic Energy Sciences, Division of Materials Science and Engineering, under Award DE-FG02-04ER46145 for single-crystal and microcrystalline syntheses; structural analyses; and PXRD, SEM, and EDS measurements and analyses. X.Z. and T.M.T. acknowledge support, in part,

DOI: 10.1021/acs.inorgchem.5b00348
Inorg. Chem. 2015, 54, 5316−5321

from a KAUST Faculty Initiated Collaboration grant and also some funding from Clemson University.

REFERENCES

(1) Kovnir, K. A.; Shevelkov, A. V. *Russ. Chem. Rev.* **2004**, *73*, 923−938.
(2) Rogl, P. In *Handbook of Thermoelectrics*; Rowe, D. M., Ed.; CRC Press: Boca Raton, FL, 2006; Chapter 32.
(3) Karttunen, A. J.; Fässler, T. F.; Linnolahti, M.; Pakkanen, T. A. *Inorg. Chem.* **2011**, *50*, 1733−1742.
(4) *The Physics and Chemistry of Inorganic Clathrates*; Nolas, G. S., Ed.; Springer: New York, 2014.
(5) He, Y.; Sui, F.; Kauzlarich, S. M.; Galli, G. *Energy Environ. Sci.* **2014**, *7*, 2598−2602.
(6) (a) Nolas, G. S.; Slack, G. A.; Schujman, S. B. *Semicond. Semimetals* **2001**, *69*, 255−300. (b) Shi, X.; Yang, J.; Bai, S.; Yang, J.; Wang, H.; Chi, M.; Salvador, J. R.; Zhang, W.; Chen, L.; Wong-Ng, W. *Adv. Funct. Mater.* **2010**, *20*, 755−763. (c) Martin, J.; Wang, H.; Nolas, G. S. *Appl. Phys. Lett.* **2008**, *92*, 222110.
(7) Chaturvedi, A.; Stefanoski, S.; Phan, M.-H.; Nolas, G. S.; Srikanth, H. *Appl. Phys. Lett.* **2011**, *99*, 162513.
(8) (a) Shevelkov, A. V.; Kovnir, K. A. *Struct. Bonding (Berlin)* **2011**, *139*, 97−142. (b) Prokofiev, A.; Sidorenko, A.; Hradil, K.; Ikeda, M.; Svagera, R.; Waas, M.; Winkler, H.; Neumaier, K.; Paschen, S. *Nat. Mater.* **2013**, *12*, 1096−1101.
(9) (a) Stefanoski, S.; Beekman, M.; Wong-Ng, W.; Zavalij, P.; Nolas, G. S. *Chem. Mater.* **2011**, *23*, 1491−1495. (b) Stefanoski, S.; Nolas, G. S. *Cryst. Growth Des.* **2011**, *11*, 4533−4537. (c) Rachi, T.; Tanigaki, K.; Kumashiro, R.; Winter, J.; Kuzmany, H. *Chem. Phys. Lett.* **2005**, *409*, 48−51.
(10) (a) Munir, Z. A.; Anselmi-Tamburini, U.; Ohyanagi, M. *J. Mater. Sci.* **2006**, *41*, 763−777. (b) Orru, R.; Licheri, R.; Locci, A. M.; Cincotti, A.; Cao, G. *Mater. Sci. Eng.* **2009**, *R 63*, 127−287. (c) Suarez, M.; Fernandez, A.; Menendez, J. L.; Torrecillas, R.; Kessel, H. U.; Hennicke, J.; Kirchner, R.; Kessel, T. Challenges and Opportunities for Spark Plasma Sintering: A Key Technology for a New Generation of Materials. In *Sintering Applications*; Ertug, B., Ed.; InTech: Rijeka, Croatia, 2013; pp 319−342.
(11) Beekman, M.; Baitinger, M.; Borrmann, H.; Schnelle, W.; Meier, K.; Nolas, G. S.; Grin, Yu. *J. Am. Chem. Soc.* **2009**, *131*, 9642−9643.
(12) Stefanoski, S.; Blosser, M. C.; Nolas, G. S. *Cryst. Growth Des.* **2013**, *13*, 195−197.
(13) Baran, V.; Senyshyn, A.; Karttunen, A. J.; Fischer, A.; Scherer, W.; Raudaschl-Sieber, G.; Fässler, T. F. *Chem.—Eur. J.* **2014**, *20*, 1−13.
(14) (a) Larson, A. C.; Von Dreele, R. B. *General Structure Analysis System*; Report LAUR 86-748; Los Alamos National Laboratory: Los Alamos, NM, 2004. (b) Toby, B. H. *J. Appl. Crystallogr.* **2001**, *34*, 210−221.
(15) *APEX2*; Bruker AXS Inc.: Madison, WI, 2010.
(16) *SAINT Data Reduction Software*; Bruker AXS Inc.: Madison, WI, 2009.
(17) Sheldrick, G. M. *SADABS. Program for Empirical Absorption Correction*; University of Göttingen: Göttingen, Germany, 2008.
(18) Sheldrick, G. M. *SHELXS-97 and SHELXL-97*; University of Göttingen: Göttingen, Germany, 1998.
(19) Farrugia, L. J. *J. Appl. Crystallogr.* **1999**, *32*, 837−838.
(20) Kortüm, G. *Reflectance Spectroscopy*; Springer: New York, 1969.
(21) Witte, J.; von Schnering, H. G. *Z. Anorg. Allg. Chem.* **1964**, *327*, 260.
(22) Westerhaus, W.; Schuster, H. U. *Z. Naturforsch. B* **1979**, *34*, 352.
(23) Roudebush, J. H.; de la Cruz, C.; Chakoumakos, B. C.; Kauzlarich, S. M. *Inorg. Chem.* **2012**, *51*, 1805−1812.
(24) Shannon, R. D. *Acta Crystallogr. A* **1976**, *32*, 751−767.
(25) Adams, G. B.; O'Keeffe, M.; Demkov, A. A.; Sankey, O. F.; Huang, Y.-M. *Phys. Rev. B* **1994**, *49*, 8048−8053.
(26) Kittel, C. *Introduction to Solid State Physics*, 8th ed.; John Wiley & Sons: New York, 2005; p190.
(27) Imai, M.; Sato, A.; Udono, H.; Imai, Y.; Tajima, H. *Dalton Trans.* **2011**, *40*, 4045−4047.
(28) Condron, C. L.; Martin, J.; Nolas, G. S.; Piccoli, P. M. B.; Schultz, A. J.; Kauzlarich, S. M. *Inorg. Chem.* **2006**, *45*, 9381−9386.
(29) Mudryk, Y.; Rogl, P.; Paul, C.; Berger, S.; Bauer, E.; Hilscher, G.; Godart, C.; Noël, H. *J. Phys.: Condens. Matter* **2002**, *14*, 7991−8004.
(30) (a) Nolas, G. S.; Ward, J. M.; Gryko, J.; Qiu, L.; White, M. A. *Phys. Rev. B* **2001**, *64*, 153201. (b) Stefanoski, S.; Martin, J.; Nolas, G. S. *J. Phys.: Condens. Matter* **2010**, *22*, 485404.
(31) Sui, F.; He, H.; Bobev, S.; Zhao, J.; Osterloh, F. E.; Kauzlarich, S. M. *Chem. Mater.* **2015**, *27*, 2812−2820.
(32) Imai, M.; Singh, S. K.; Nishio, M.; Yamada, T.; Yamane, H. *Jpn. J. Appl. Phys.* **2015**, *54*, 07JC02.

DOI: 10.1021/acs.inorgchem.5b00348
Inorg. Chem. 2015, 54, 5316−5321